water

MDPI

Article

Energy Balance, CO_2 Balance, and Meteorological Aspects of Desertification Hotspots in Northeast Brazil

Any Caroline Silva [1,*], Keila Rêgo Mendes [1], Cláudio Moisés Santos e Silva [1], Daniele Torres Rodrigues [2], Gabriel Brito Costa [1,3], Duany Thainara Corrêa da Silva [4], Pedro Rodrigues Mutti [1], Rosaria Rodrigues Ferreira [1] and Bergson Guedes Bezerra [1]

[1] Department of Atmospheric and Climate Sciences, Federal University of Rio Grande do Norte, Natal 59078-970, RN, Brazil; keila.inpa@gmail.com (K.R.M.); claudiom8@gmail.com (C.M.S.e.S.); gabrielbritocosta@gmail.com (G.B.C.); pedromutti@gmail.com (P.R.M.); rosa.meteoro.ferreira@gmail.com (R.R.F.); bergson.bezerra@gmail.com (B.G.B.)
[2] Department of Statistic, Federal University of Piauí, Teresina 64049-550, PI, Brazil; mspdany@gmail.com
[3] Institute of Biodiversity and Forests, Federal University of Western Pará, Santarém 68035-110, PA, Brazil
[4] Institute of Engineering and Geosciences, Federal University of Western Pará, Santarém 68035-110, PA, Brazil; duanythaynara@gmail.com
* Correspondence: anycarolinen@hotmail.com

Abstract: The main objective of this study was to evaluate meteorological variables and the simulated components of energy and CO_2 balances in desertification hotspots in Northeast Brazil. Meteorological data were obtained from the National Institute of Meteorology measurement network for the Cabrobó and Ibimirim sites. Initially, hourly linear trends were calculated for the meteorological variables using the non-parametric Mann–Kendall test. Then, the seasonal variability in the components of energy and CO_2 balances was assessed through simulations of the simple tropical ecosystem (SITE) model. Results showed evidence of increasing air temperature trends in the Cabrobó site in the first months of the year, which was not observed in the Ibimirim site. Regarding relative humidity, increasing trends were observed in a few months over the Cabrobó site, while decreasing trends were observed in the Ibimirim site. Opposite behaviors were also identified for the trends in wind speed in both sites. Gross primary production (GPP) and net ecosystem exchange (NEE) simulated values were higher in the first half of the year in both sites. GPP varied from 0.8 to 1.2 g C m^{-2} h^{-1}, and NEE fluctuated around approximately −5 g C m^{-2} h^{-1}. These results indicate that rainfall seasonality is a crucial factor for the modulation of CO_2 and energy balance fluxes in the Caatinga biome.

Keywords: microclimate; land degradation; atmosphere–biosphere interaction; modeling

check for updates

Citation: Silva, A.C.; Rêgo Mendes, K.; Santos e Silva, C.M.; Torres Rodrigues, D.; Brito Costa, G.; Thainara Corrêa da Silva, D.; Rodrigues Mutti, P.; Rodrigues Ferreira, R.; Guedes Bezerra, B. Energy Balance, CO_2 Balance, and Meteorological Aspects of Desertification Hotspots in Northeast Brazil. *Water* **2021**, *13*, 2962. https://doi.org/10.3390/w13212962

Academic Editor: Luis Garrote

Received: 31 August 2021
Accepted: 12 October 2021
Published: 20 October 2021

Publisher's Note: MDPI stays neutral with regard to jurisdictional claims in published maps and institutional affiliations.

Copyright: © 2021 by the authors. Licensee MDPI, Basel, Switzerland. This article is an open access article distributed under the terms and conditions of the Creative Commons Attribution (CC BY) license (https://creativecommons.org/licenses/by/4.0/).

1. Introduction

Desertification can be described as the persistent degradation of the biophysical environment of drylands, caused either by human-induced processes or climate variability [1–3]. The United Nations Convention to Combat Desertification [1] acknowledges it as one of the major environmental problems worldwide, and the associated impacts are estimated to affect up to 250 million people [1,4]. Desertification poses an even bigger threat to already vulnerable arid and semiarid regions, where the local population is usually highly dependent on natural resources, and therefore, land degradation furthers hampers development [5–7]. Furthermore, future climate change scenarios indicate an overall increase in the frequency and intensity of climate extreme events such as droughts, which may accelerate desertification processes over drylands [8].

In South America, the Northeast Brazil (NEB) region encompasses some of the most vulnerable semiarid regions in the continent [9]. Indeed, studies in the NEB already indicate a reduction in rainfall volumes and an expansion of its arid and semiarid domains [10–12].

Additionally, degraded lands in the NEB are expanding due to increasing firewood production and poor soil management and agriculture practices (slash and burn), which cause deforestation, soil salinization, and ultimately desertification [4,13].

The rapid intensification of desertification in the NEB is responsible for the suppression of the Caatinga vegetation, a highly biodiverse, exclusively Brazilian seasonally dry tropical forest, characterized mainly by thorny deciduous species [14]. The degradation of the Caatinga biome may play a fundamental role in the formation and expansion of desertification hotspots in the NEB, as previously reported by others [4,13,15]. Therefore, it is of extreme significance to study and quantify the impacts of desertification in key environmental and biophysical processes related to the native Caatinga vegetation, such as energy and CO_2 balances.

For instance, despite the systematic increase in CO_2 concentrations in the atmosphere throughout the years, terrestrial vegetated ecosystems usually behave as carbon sinks, and thus, biome-oriented studies are of the utmost importance to better understand CO_2 dynamics at the regional and global scales [16,17]. However, the interannual variability in CO_2 absorption by terrestrial carbon sinks is strongly related to rainfall, temperature, and other meteorological variables [18,19]. Recent studies showed that the Caatinga biome potentially behaves similar to a carbon sink even in dry years, but CO_2 dynamics were largely driven by meteorological conditions [20,21]. The potential impacts of desertification in the CO_2 balance of Caatinga are yet unknown.

Similarly, the energy balance analysis over vegetated surfaces allows the dimensioning of mass and energy exchanges in the soil–vegetation–atmosphere system through the partitioning of net radiation into energy processes such as latent (associated with evaporation and transpiration processes), sensible (used to heat the air), and soil (which is associated with heat diffusion in the soil) heat fluxes [22–24]. They also allow the assessment of microclimate changes over a given region due to land-use changes, as well as soil and atmosphere conditions. Therefore, landscape changes due to desertification will impact the partitioning of energy balance [25]. For example, previous studies in the Caatinga biome indicated that 50% of annual net radiation was used as sensible heat flux [24]. The expansion of desertification hotspots can further increase the portion of radiation transformed into sensible heat flux, which may impact the local and regional climate [25].

Currently, there are no studies in the scientific literature with in situ measurements of the components of these balances over desertification hotspots in the NEB, despite the undeniable environmental and social relevance of this process to the region. Thus, the objectives of the present study were (1) to evaluate the role of the different components of energy and CO_2 balances in desertification hotspots in the semiarid NEB and (2) to assess the regional dynamics of the desertification process in relation to meteorological variables measured in situ. The energy balance components (latent and sensible heat fluxes), the Bowen ratio (which is the ratio between sensible and heat fluxes), and the CO_2 balance components (gross primary production—GPP, and net ecosystem exchange—NEE) were simulated using SVAT models. To that end, we used data measured in the Cabrobó site (NEB desertification hotspot) and in the Ibimirim site (surroundings of the Cabrobó desertification hotspot) while also identifying trends in the meteorological variables measured over the two sites.

The state-of-the-art method for the evaluation of CO_2 and energy balances over vegetated environments is the use of eddy-covariance systems through high-frequency continuous measurements [26–28]. However, these systems are costly, and their installation and monitoring in desertification zones may be challenging. Therefore, biophysical soil–vegetation–atmosphere transfer (SVAT) models can be used as alternative tools to simulate the components of CO_2 and energy balance. It must be noted that both observational and modeling studies have been carried out in Brazil, mostly over the Amazon and the Cerrado biome [29]. The Caatinga biome and the NEB semiarid region, however, are still scarcely studied regarding CO_2 and energy balance, despite recent efforts [21,24,30–32].

2. Materials and Methods

2.1. Data

Meteorological data were obtained through the National Institute of Meteorology (Instituto Nacional de Meteorologia—INMET)) measuring network. The spatial distribution of the selected stations, as well as the location of the desertification hotspots in the NEB (as delimited by the National Institute for the Semiarid (INSA)) are presented in Figure 1. Air temperature (°C), relative humidity (RH%), atmospheric pressure (hPa), wind speed (m s^{-1}), global radiation (kJ m^{-2}), and rainfall (mm) data were used. They were measured every five seconds and stored as hourly means. The exception is rainfall data, which refers to hourly accumulated values. Data were available for the period from 1 January 2008 until 3 December 2018.

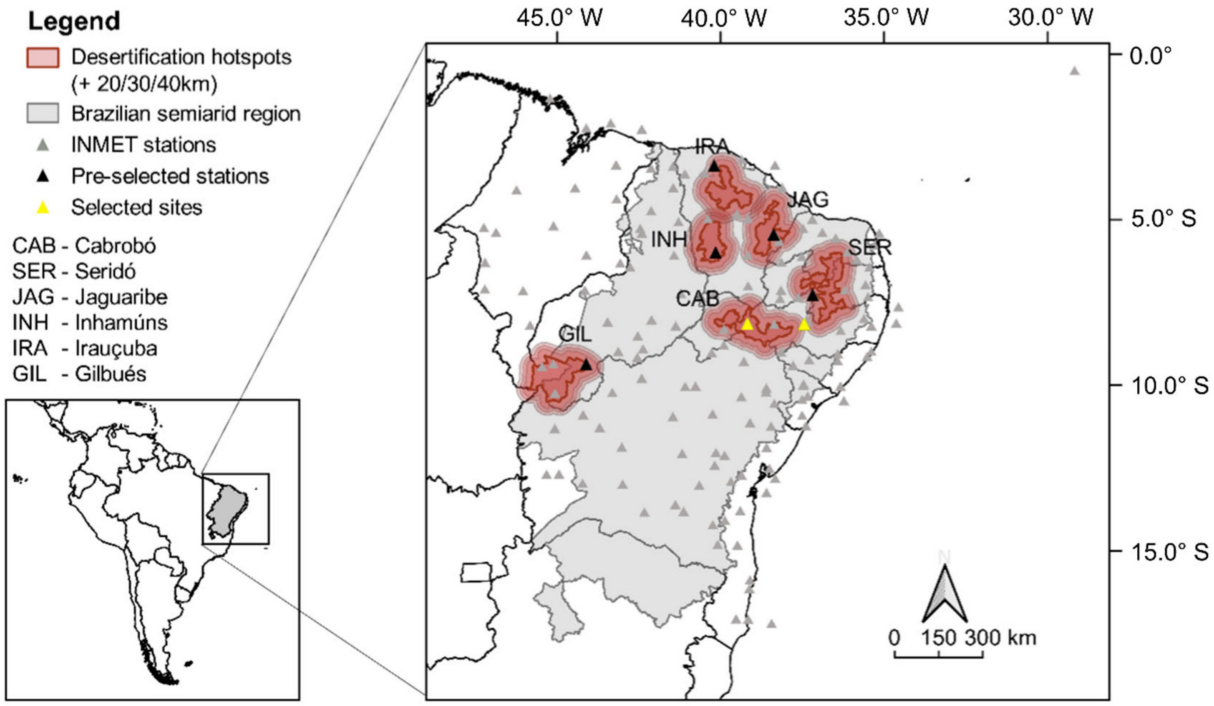


Figure 1. Spatial distribution of INMET stations and location of desertification hotspots.

2.2. Selection of the Simulation Sites

Firstly, we analyzed seven (which are the black and yellow triangles) cities located within the six NEB desertification hotspots (Figure 1). We included Ibimirim town in the analysis due to the proximity to the CAB desertification hotspots. From the Gilbués hotspot, we selected the Bom Jesus do Piauí town, located at the southern Piauí state, in a transition region between the Caatinga and Cerrado biomes. In the Irauçuba hotspot, the Sobral city was selected, located 20 km from the hotspot boundaries. The Patos town was selected for the Seridó hotspot, which is also 20 km in distance from its boundaries. For the Jaguaribe, Inhamuns, and Cabrobó desertification hotspots, the towns of Jaguaribe, Tauá, and Cabrobó were selected, which are located inside the hotspots. The coordinates, elevation, and percentage of data gaps for each selected station are presented in Table 1. Mean annual accumulated rainfall, temperature, and relative humidity are shown in Table 2. Cabrobó and Ibimirim feature the lowest mean annual precipitation values, with 404.6 and 380.9 mm/year, respectively. However, air temperature is lower in these two locations due to nighttime cooling, which is a typical phenomenon in arid regions, particularly during the drier periods of the year.

Table 1. Location of the seven municipalities located within or in the surroundings of each desertification hotspot in the NEB, as shown in Figure 1: PI, Piauí state; PE, Pernambuco state; CE, Ceará state; PB, Paraíba state.

Station	Latitude	Longitude	Elevation	Gaps
Bom Jesus do Piauí (PI)	09°04′28″ S	44°21′31″ W	277 m	7%
Cabrobó (PE)	08°30′51″ S	39°18′36″ W	325 m	3%
Ibimirim (PE)	08°32′26″ S	37°41′25″ W	395 m	2%
Jaguaribe (CE)	05°53′26″ S	38°37′19″ W	123 m	3%
Patos (PB)	07°01′28″ S	37°16′48″ W	242 m	7%
Sobral (CE)	03°41′10″ S	40°20′59″ W	69 m	15%
Tauá (CE)	06°00′11″ S	40°17′34″ W	402 m	3%

Table 2. Averages of climate variables of the seven municipalities according to Table 1.

Averages of Climate Variables			
Station	**Annual Accumulated Precipitation (mm)**	**Air Temperature (°C)**	**Relative Humidity (%)**
Bom Jesus do Piauí (PI)	598.1	27.3	62.3
Cabrobó (PE)	407.6	27.1	59.1
Ibimirim (PE)	380.9	25.9	59.1
Jaguaribe (CE)	407.8	29.1	55.0
Patos (PB)	654.6	27.9	52.0
Sobral (CE)	505.1	27.6	69.0
Tauá (CE)	507.5	27.1	55.9

These seven stations were primarily analyzed regarding (i) data quality, prioritizing stations with fewer data gaps; (ii) proximity to the desertification hotspot, prioritizing stations located within hotspots; (iii) proximity of other nearby stations in the surroundings of the hotspots that could be used as comparison regarding the response of each observed and simulated data. By adopting these criteria, the Cabrobó site was selected for the simulations and meteorological data analysis, with the Ibimirim station being used for comparison (Table 1). Both sites are located in the Pernambuco state; the Cabrobó site is located within the Cabrobó desertification hotspot (Figure 1), and the Ibimirim site is located approximately 40 km from the boundaries of the hotspot and 190 km from the Cabrobó site. The selected hotspot and sites are located south of the Pernambuco state, in a region highly dependent on agriculture, which can be directly affected by the consequences of desertification, economically impacting the entire region [33].

2.3. Soil–Vegetation–Atmosphere Transfer Model

In order to determine the components of energy and CO_2 balances, we used the simple tropical ecosystem (SITE) model, which represents soil–vegetation–atmosphere processes and was first designed as a tool to be used in tropical ecosystems [34]. The SITE model comprises different surface processes such as infrared radiation budget above the canopy, solar radiation budget, aerodynamic processes, canopy physiology and transpiration, canopy water budget, mass and energy transfer in the atmosphere, two-layer soil heat fluxes, soil water, carbon flux, and balance.

There is a great variety of available models similar to SITE [29], as reported in another study. However, for this particular study, the SITE model is more advantageous because it has been previously calibrated for the Caatinga environment [31], presenting satisfactory results, with correlation coefficients statistically significant at a 95% confidence level, which is higher than 0.70 for energy and CO_2 balance components. These results were obtained through the assimilation of in situ measurements of biome information such as specific leaf area, leaf width, maximum capacity of rubisco enzyme, coefficient of stomatal conductance,

etc. Thus, the same specific parametrization used in another study [31] was used in the simulations of this study.

In order to more objectively represent results, we selected two contrasting years regarding annual rainfall volumes, since it is the main meteorological aspect driving ecosystem activity in the region. The choice of the years was based on another study [2], which evaluated vegetation–rainfall relations in NEB desertification hotspots and showed that 2009 was an anomalously wet year and 2014 was an anomalously dry year in the Cabrobó hotspot. Table 3 shows the annual accumulated rainfall and its anomalies during the period from 2008 to 2018. The anomalies were calculated by subtracting each annual value from the 2008–2018 average. We can observe that in 2009 the anomalies were most intense in both Cabrobó and Ibimirim, but during 2014, the anomalies were lower than in 2012 or 2017. It is worth mentioning that the 2014 dataset presented fewer gaps than the other years, and an ongoing intense drought episode was established in 2012. Therefore, each simulation started at 00:00 UTC on 1 January of each respective year and ended at 23:00 UTC on 31 December of each selected year.

Table 3. Annual accumulated rainfall and annual anomalies to the period from 2008 to 2018 in Cabrobó and Ibimirim.

	Annual Rainfall Accumulated (mm)		Annual Rainfall Anomalies (mm)	
Years	**Cabrobó**	**Ibimirim**	**Cabrobó**	**Ibimirim**
2009	747.5	724.4	367.9	311.2
2010	502.0	835.6	122.4	422.4
2011	562.2	560.8	182.6	147.6
2012	207.6	147.0	−172.0	−266.2
2013	321.2	338.2	−58.4	−75.0
2014	229.4	307.8	−150.2	−105.4
2015	241.4	285.4	−138.2	−127.8
2016	386.2	327.8	6.6	−85.4
2017	224.4	264.0	−155.2	−149.2
2018	373.8	341.4	−5.8	−71.8

The SITE model uses six input meteorological variables (hourly samples) as initial conditions: rainfall (mm), air temperature (°C), specific humidity (g kg^{-1}), wind speed (m s^{-1}), global radiation (W m^{-2}), and longwave radiation emitted by the atmosphere (W m^{-2}). Output variables simulated by the model are net radiation (R_n) photosynthetically active radiation (PAR), soil heat flux (G), sensible heat flux (H), latent heat flux (LE), net CO_2 exchange (NEE), net primary production (NPP), gross primary production (GPP), the fraction of absorbed photosynthetically active radiation (FAPAR), and leaf area index (LAI).

Rainfall, air temperature, atmospheric pressure, wind speed, and global radiation are directly measured at INMET stations. Specific humidity (q) and longwave radiation emitted by the atmosphere ($L\downarrow$ were calculated based on classic methods that will be described in the following sections.

2.3.1. Specific Air Humidity Calculation

Specific air humidity is defined as the mass of water vapor in a unit of air mass (kg kg^{-1} or g kg^{-1}) and can be calculated by using RH, air temperature, and atmospheric pressure data [35]. RH is the ratio between partial water vapor pressure (e) and water vapor saturation pressure (e_s). Thus,

$$RH = \frac{e}{e_s} \times 100 \quad (1)$$

where e_s is determined by the Tetens equation as follows:

$$e_s = 6.1078 \times 10^{\frac{7,5\ T}{237.3+T}} \quad (2)$$

where T (°C) is air temperature. Then, we calculate e as follows:

$$e = \frac{RH \times e_s}{100} \quad (3)$$

and finally, specific humidity is determined by the following equation:

$$q = \frac{0.622\ e}{P - 0.378\ e} \quad (4)$$

where P (hPa) is the atmospheric pressure directly measured at the INMET station.

2.3.2. Longwave Radiation Emitted by the Atmosphere

Longwave radiation emitted by the atmosphere was calculated through the Stefan–Boltzmann law, in which the emissivity of a body is proportional to the fourth power of the absolute temperature of said body. Thus,

$$L\downarrow = \varepsilon_a\ \sigma\ T^4 \quad (5)$$

where $\sigma = 5.67 \times 10^{-8}$ W m^{-2}K^{-4} is the Stefan–Boltzmann constant, and ε_a is the atmospheric emissivity, which was calculated through two empirical models proposed by Idso [36] (Equation (6)) and Prata [37] (Equation (7)), respectively.

The choice of these two models was based on previous analyses carried out in the Caatinga and Cerrado biomes [38–40]. Although these studies used different methods, they all agreed in indicating the models by Idso [36] and Prata [37] as appropriate in order to better represent atmospheric emissivity in the region. Specifically, a study [40] was carried out using in situ eddy covariance data measured in a preserved Caatinga segment. The same dataset was used in the calibration of the SITE model [31]. The quality of these data was previously analyzed and verified in other studies [21,24,30].

Idso's model [36] determines emissivity through observed air temperature data and estimated vapor pressure (Equation (6)). Similarly, Prata's model [37] determines emissivity based on air temperature and partial water vapor pressure (Equation (7)).

$$\varepsilon_{a,6} = 0.70 + 5.95 \times 10^{-7} \times e \times exp\left(\frac{1500}{T}\right) \quad (6)$$

$$\varepsilon_{a,7} = \left\{1 - (1 + \xi)exp\left[-(1.2 + 3.0\xi)^{0.5}\right]\right\}, with\ \xi = 0.465\left(\frac{e}{T}\right) \quad (7)$$

Although both models performed well in representing observed data, the model by Prata was slightly more advantageous regarding the mean absolute error [40]. Thus, we attributed weights to the emissivity computed by each model, with a 0.6 weight to Prata's model and a 0.4 weight to Idso's model. Finally, we calculated longwave radiation emitted by the atmosphere as follows:

$$L\downarrow = (0.4\varepsilon_{a.6} + 0.6\varepsilon_{a.7})\sigma\ T^4 \quad (8)$$

Since measured $L\downarrow$ data at the Ibimirim and Cabrobó sites are not available, the weighed emissivity solution (Equation (8)) was used in order to minimize errors inherent to the empirical nature of the formulations used for the calculation of the emissivity parameter.

2.4. Statistical Analysis

Linear trends were calculated by the non-parametric Mann–Kendall trend test [41,42]. This test consists of a comparison of each value of the time series with the remaining

sequential values, calculating the number of times the remaining values are higher than the current tested value. The non-parametric Mann–Kendall trend test has been vastly used in trend analysis studies of meteorological variables in the NEB [43–45]. The following different statistical significance levels were used: 0.001, 0.01, 0.05, and 0.1 *p*-values. Trends tests were used for the entire air temperature, relative air humidity, and wind speed data series (January 2008 to December 2018). The results were analyzed as hourly trends and therefore are unprecedented to the region.

The statistical analyses were carried out in the R software [46], and figures were generated using the ggplot2 package [47]. Boxplots were used because they simultaneously represent different important statistical aspects of data, such as central tendency, variability, symmetry, and the presence of outliers. The boxplot shows three quartiles, and the minimum and maximum data in a vertically aligned rectangular box. The box comprises the interquartile interval, with its lower limit representing the first quartile (Q1) and its upper limit representing the third quartile (Q3). A dashed line within the box represents the second quartile (median). In both extremes of the box, there is a vertical line extending towards the maximum and minimum observed values. These are the so-called whiskers that extend to a distance of 1.5 from the limits of the box (Q3-Q1) (Chambers et al. (1983)). All data beyond these limits are highlighted as outliers (values lying too far from the majority), represented by blank circles. In addition, the mean value was also added to the boxplot represented by a filled circle.

3. Results

3.1. Seasonal Variability in Observed Meteorological Variables

Figure 2 shows the observed monthly rainfall variability in Cabrobó and Ibimirim in the years 2009 (wet year) and 2014 (dry year). In the wet year, Cabrobó registered higher rainfall volumes in all five initial months of the year, with the exception of May, when Ibimirim registered higher values. In the following months, both sites presented similar rainfall variability, with low precipitation volumes (0 to 50 mm) due to the establishment of the dry season. In December 2009, a rainfall peak (120 mm) can be observed in Ibimirim due to an early onset of the rainy season of the subsequent year (2010). In the dry year (2014), monthly rainfall values did not exceed 50 mm in Cabrobó. Similar behavior was observed in Ibimirim, with the exception of February, when more than 100 mm of precipitation was registered.

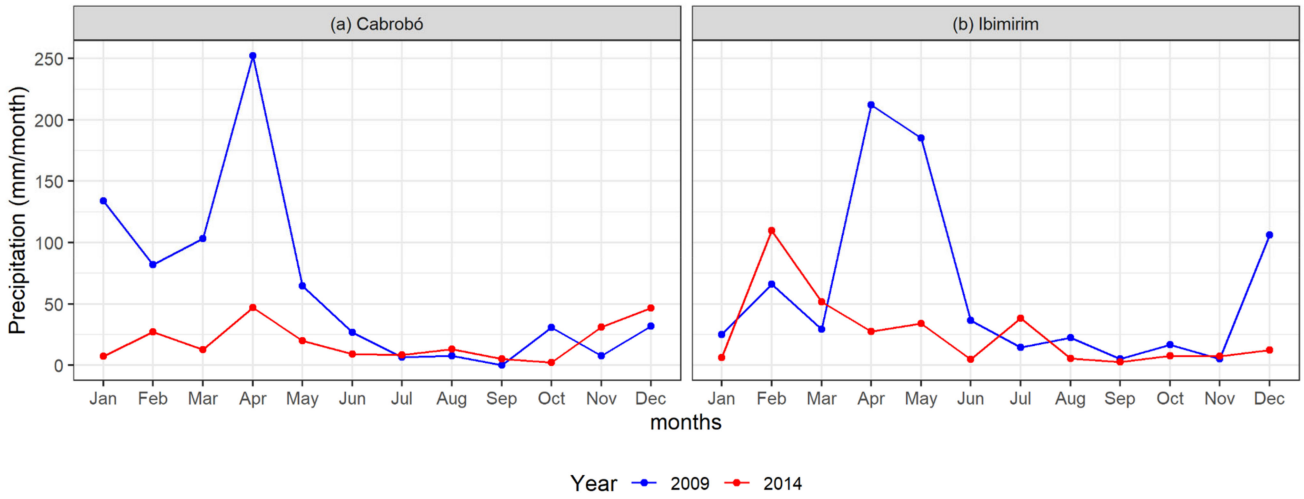


Figure 2. Observed monthly rainfall variability in Cabrobó and Ibimirim in 2009 (wet year) and 2014 (dry year).

Figure 3 shows the air temperature in both studied sites and in the two contrasting years (2009 and 2014). In the wet season (first five months of the year), both sites present a similar air temperature behavior, but in the months from May to August, temperatures in

Cabrobó were relatively higher, compared with Ibimirim, with the lowest values reaching 24 °C in Cabrobó and 22 °C in Ibimirim. Nevertheless, months with the highest and lowest temperatures coincided in both sites. In the dry period, the variability of air temperature was similar in both sites, but Cabrobó values exceeded 28 °C from September through December, while in Ibimirim, it only occurred in November.

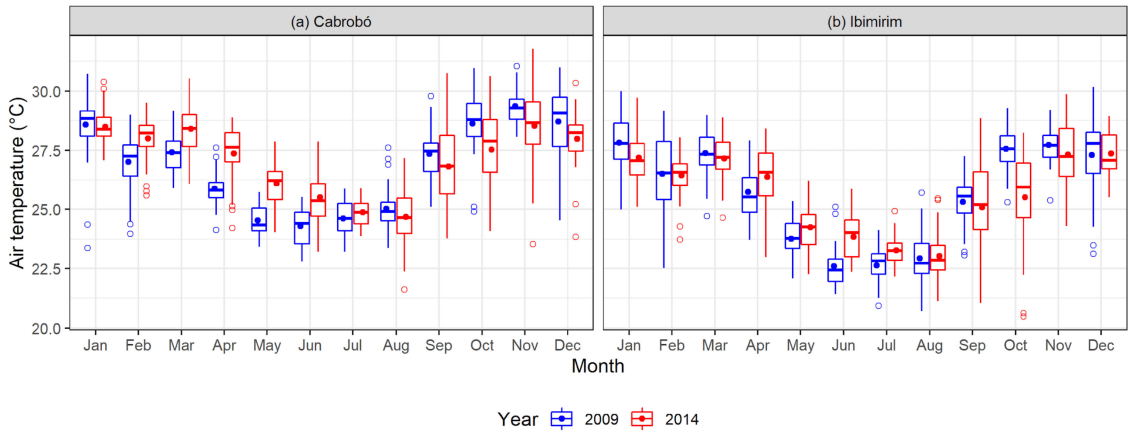


Figure 3. Monthly boxplots of hourly air temperature data in the Cabrobó and Ibimirim sites in 2009 (wet year) and 2014 (dry year).

In Cabrobó, the mean air temperature was higher in 2014 between February and June, than in 2009, which reflects the lower observed monthly precipitation. On the other hand, in Ibimirim, the mean air temperature was higher in 2014 during the months from April to July, confirming the influence of monthly rainfall distribution on temperature over the region. In the dry months (September to December), the temperature in 2014 presented a higher variability than in 2009, with temperature values lower than 21.5 °C (outliers) registered in Ibimirim, indicating that despite the lower annual accumulated rainfall that year, anomalous rainfall events can still drive the decrease in temperature.

Relative air humidity observed in Cabrobó and Ibimirim in 2009 and 2014 is shown in Figure 4. In the rainy season, both sites presented a similar monthly variability, with the highest RH value occurring in May. Additionally, higher RH values were observed during the five initial months of the years. In the dry season, Ibimirim presented higher RH values (greater than 80%), compared with Cabrobó, while also presenting a larger range in observed values.

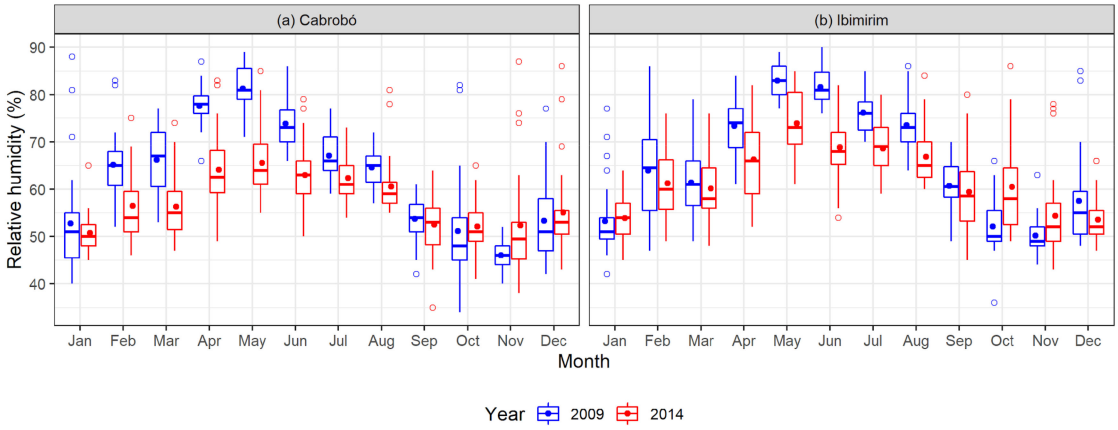


Figure 4. Monthly boxplots of hourly relative humidity data in the Cabrobó and Ibimirim sites in 2009 (wet year) and 2014 (dry year).

Figure 5 shows the monthly wind speed variability in Cabrobó and Ibimirim, in 2009 and 2014. In the rainy season, wind speed varied from 1.0 to 5.0 m s^{-1} in Cabrobó, while in Ibimirim, the range was smaller, with values between approximately 2.0 and 4.0 m s^{-1}. In the dry season, Cabrobó also presented higher wind speed values, with observations ranging from 2.0 to 5.0 m s^{-1}, while in Ibimirim, values ranged from 2.0 to 4.0 m s^{-1}.

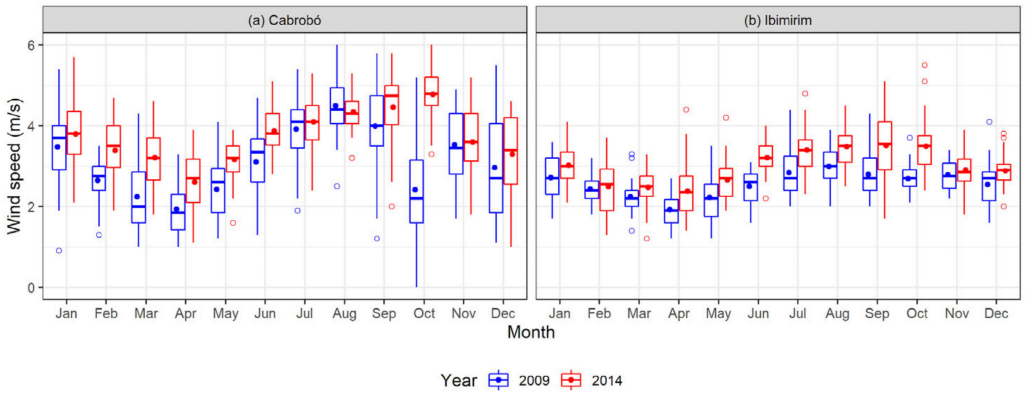


Figure 5. Monthly boxplots of hourly wind speed data in the Cabrobó and Ibimirim sites in 2009 (wet year) and 2014 (dry year).

3.2. Hourly Linear Trends

In Figure 6a,b, the results of the Mann–Kendall test for air temperature in the Cabrobó and Ibimirim sites, respectively, are shown. In Cabrobó, statistically significant trends were identified between 20:00 and 08:00, indicating increasing air temperatures during the night from December to August, which comprises the entire wet season in the region. On the other hand, no statistically significant trend was identified in the drier months (September to November). In Ibimirim, only a few sparsely distributed hours presented statistically significant trends. Despite the noticeable increase in temperature in Cabrobó (within the desertification hotspot), there were no significant temperature changes in Ibimirim (in the surroundings of the hotspot).

Trends results for relative humidity in both sites are shown in Figure 6c,d. In Ibimirim, increasing relative humidity trends were identified between August and October, mainly during night hours. In Cabrobó, however, an increasing trend was observed during the day from October to December, while sporadic negative trends were identified during the night from July to September.

In Figure 6e,f, the results of the Mann–Kendall test are shown regarding wind speed data in both sites. In Cabrobó, only March and April did not present significant trends. From May to June, significant decreasing wind speed trends were observed mostly from 9h to 11h. In the second half of the year (July to December), decreasing trends were identified during almost all hours of the day, especially from July to September, in which the results presented high statistical significance. In Ibimirim (Figure 6f), an opposite behavior was observed, compared with Cabrobó. The most significant trends were identified in the six initial months of the year and indicated an increase in wind speed instead of a decrease. From August until the end of the year, significant trends were also identified mostly for the period from 12 h to 24 h.

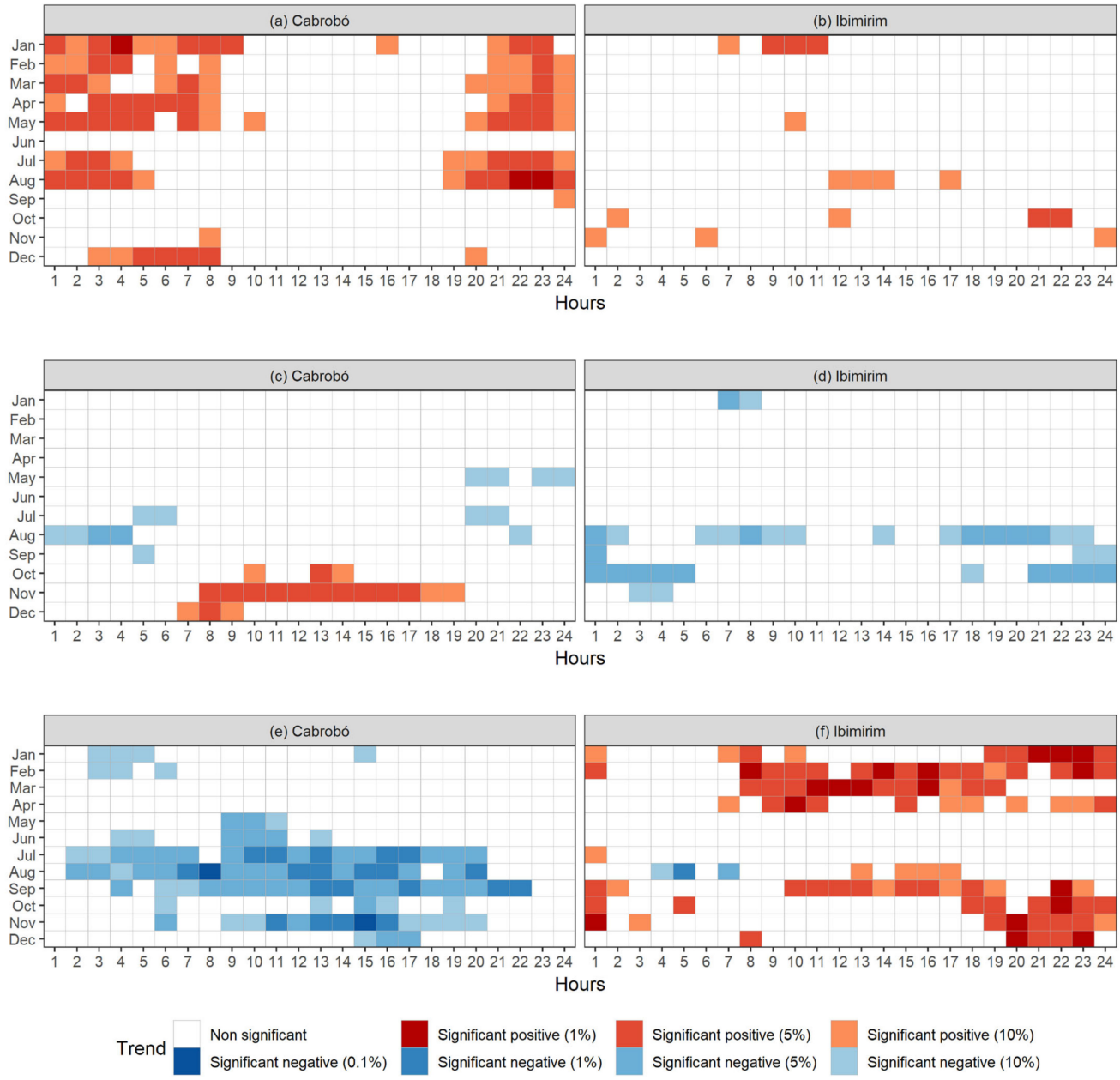


Figure 6. Hourly linear trends for air temperature (**a**,**b**), relative humidity (**c**,**d**), and wind speed (**e**,**f**). The first column refers to the Cabrobó site, and the second column refers to the Ibimirim site.

3.3. Simulated Components of Energy Balance

Figure 7 shows the monthly boxplots of simulated sensible heat flux (H) for the years 2009 and 2014 in each studied site. As it can be observed, the variability of H in the wet season is higher, ranging from 0 to 150 W m^{-2}. In the dry season, however, they ranged from negative values up to 100 W m^{-2}. Furthermore, both sites featured a similar monthly distribution of H in both years, despite Cabrobó's series presenting a slightly more accentuated variability, with extreme values (outliers) registered throughout the year, particularly from October to December (both in 2009 and 2014).

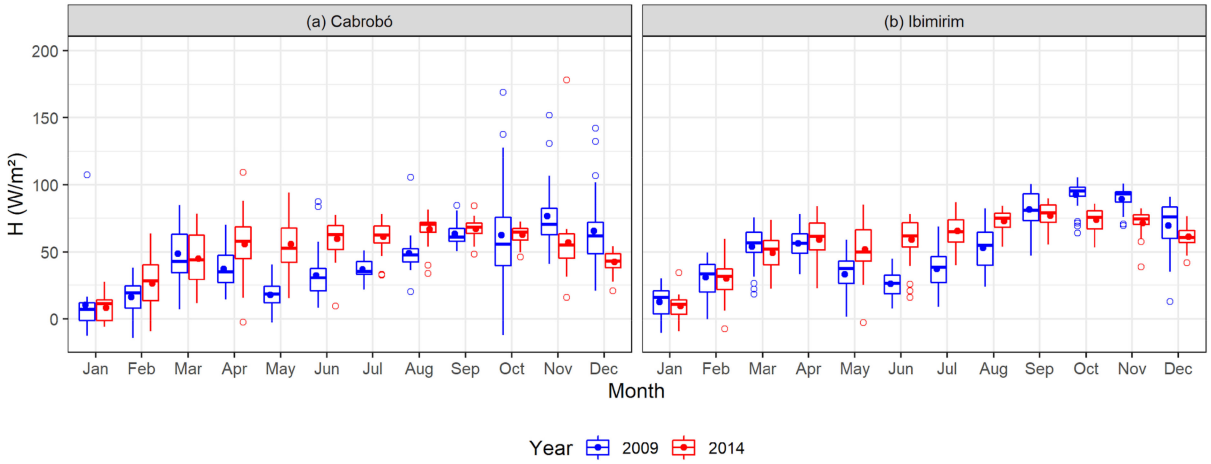


Figure 7. Monthly boxplots of hourly simulated sensible heat flux (H) in the Cabrobó and Ibimirim sites in 2009 (wet year) and 2014 (dry year).

The boxplots for the simulated latent heat flux (LE) in both sites for the years 2009 and 2014 are presented in Figure 8. Results show that the variability in LE in 2009 was higher than in 2014, in both sites. However, the simulated LE for the Cabrobó site presented a more remarkable variability, with values ranging from 0 to 450 W m^{-2} in the dry season and from 0 to 400 W m^{-2} in the wet season. Furthermore, the highest LE values were also found in Cabrobó, which reached up to 450 W m^{-2}. In both analyzed years, the values were higher during the initial three months of the year, which is expected due to the higher occurrence of rainfall these months. In 2009 and in 2014, in both sites, LE values decreased throughout the year with the establishment of the dry season, reaching the lowest values and variability in November and December.

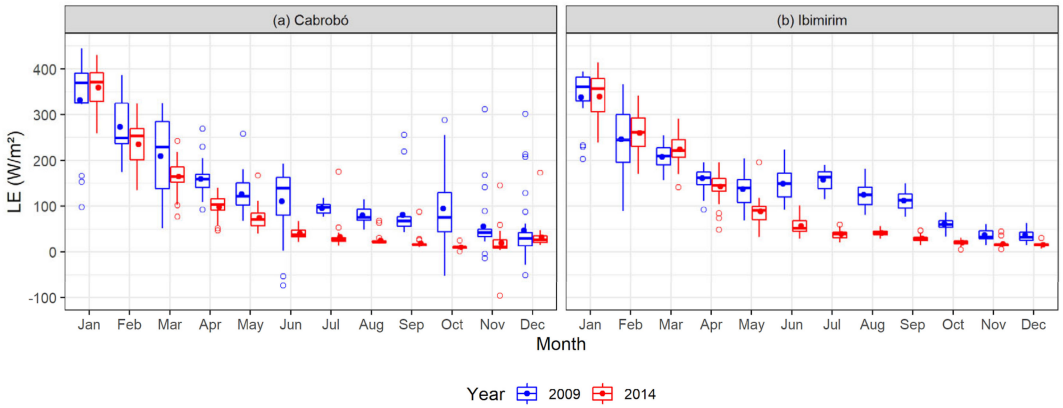


Figure 8. Monthly boxplots of hourly simulated latent heat flux (LE) in the Cabrobó and Ibimirim sites in 2009 (wet year) and 2014 (dry year).

Figure 9 shows the monthly boxplots of the Bowen ratio (ratio between H and LE) calculated for each site and year. In 2009, the Bowen ratio was small (near 0) in both sites during the initial months of the year, with no remarkable variability. In October, the Bowen ratio and its variability sharply rose, reaching up to 5.0. In 2014, however, there was a gradual increase in the Bowen ratio throughout the year, which also peaked in the last three months of the year. In December, the ratio decreased roughly 60% in Cabrobó and 15% in Ibimirim.

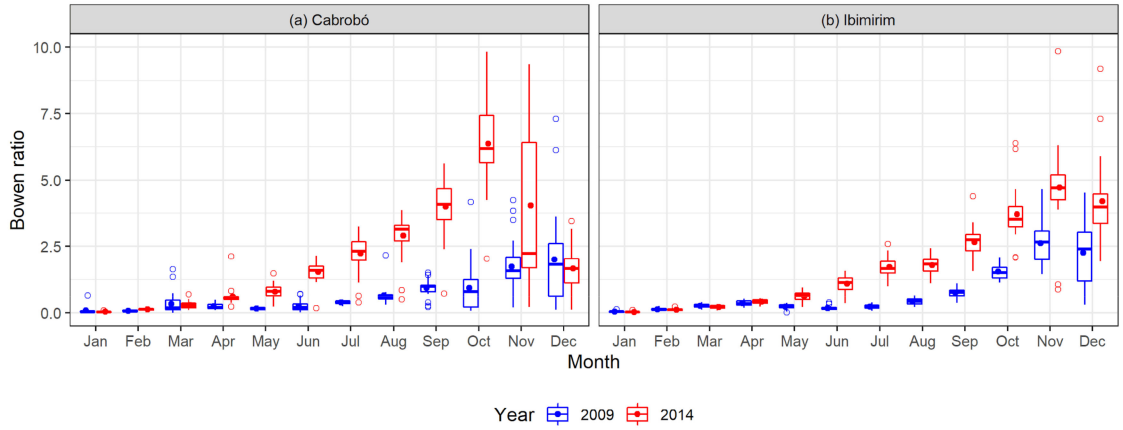


Figure 9. Monthly boxplots of hourly simulated Bowen ratio (ratio between sensible heat flux and latent heat flux) in the Cabrobó and Ibimirim sites in 2009 (wet year) and 2014 (dry year).

3.4. Simulated Components of CO_2 Balance

Boxplots of monthly values of gross primary production (GPP) are shown in Figure 10. In 2009, the simulated values ranged from 0.8 to 1.2 g C m^{-2} h^{-1} in the wet season and from 0.4 to 1.0 g C m^{-2} h^{-1} in the dry season, agreeing with the observed rainfall distribution. In 2014, GPP peaked in January in both sites, reaching values of approximately 1.2 g C m^{-2} h^{-1}, followed by a gradual linear decrease in its values, reaching its lowest values (0.3 g C m^{-2} h^{-1}) in December.

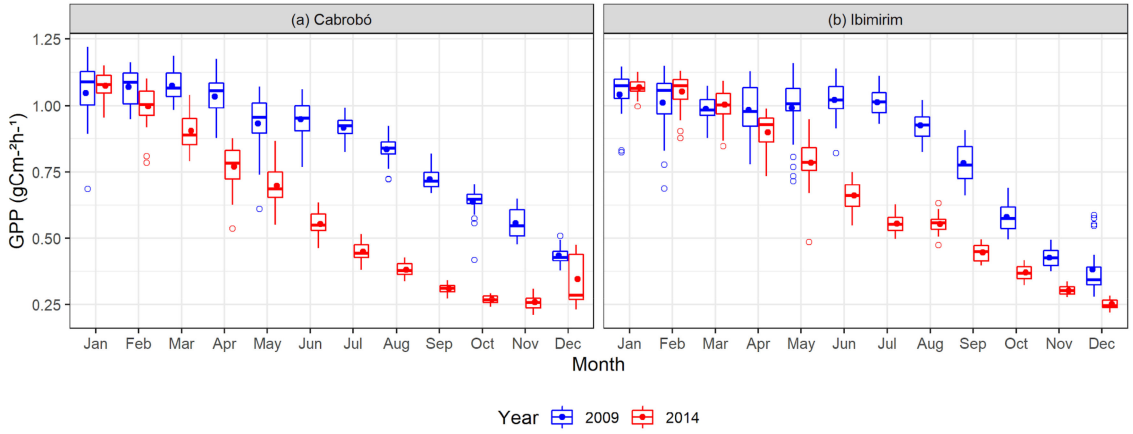


Figure 10. Monthly boxplots of hourly simulated gross primary production (GPP) in the Cabrobó and Ibimirim sites in 2009 (wet year) and 2014 (dry year).

Figure 11 shows the monthly boxplots of simulated net ecosystem exchange (NEE) for Cabrobó and Ibimirim in 2009 and 2014. One can observe that the behavior of simulated NEE is the opposite of simulated GPP, given that the more negative is the NEE, the higher is the carbon uptake. Lower NEE values (approximately -4 g C m^{-2} h^{-1}) were found in the six initial months of 2009, when more carbon is absorbed by the ecosystem. From July onward, NEE values increased, indicating a reduction in CO_2 sequestration and a clear seasonal pattern. An increase in NEE values could also be observed in 2014, although with a more linear characteristic, reaching up to 1 g C m^{-2} h^{-1} at the final trimester of the year, indicating that the release of CO_2 (ecosystem respiration) was higher than its absorption. In the wet season of 2009 (wet year), carbon uptake was higher in the first six months of the year, compared with 2014 (dry year).

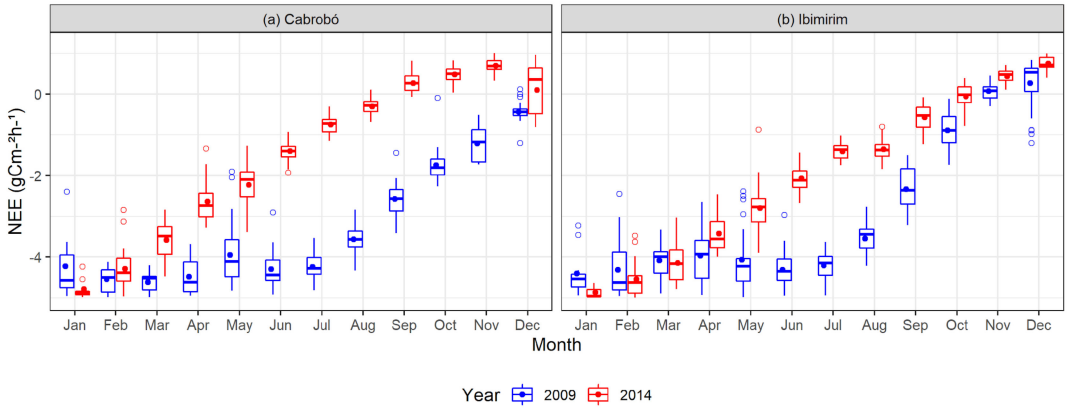


Figure 11. Monthly boxplots of hourly simulated net ecosystem exchange (NEE) in the Cabrobó and Ibimirim sites in 2009 (wet year) and 2014 (dry year). Regarding NEE values, negative values represent carbon uptake, while positive values represent carbon release.

4. Discussion

Comprehending the complex relationships between environmental factors and the components of energy and mass (CO_2) balances is crucial to combat the effects and expansion of desertification. In this study, the seasonal impact of the desertification process in meteorological variables measured in situ and in components of energy and CO_2 balances simulated by an SVAT model in NEB desertification hotspots was analyzed. Our results showed that despite the Cabrobó and Ibimirim sites being located within or near desertification hotspots under the influence of the same type of climate, meteorological variables behaved differently in each site. This is probably a consequence of the different partitioning of the energy balance at the surface.

In a region characterized by more degraded land (Cabrobó), sensible heat fluxes are expected to be higher than in less degraded lands (Ibimirim), while latent heat fluxes are expected to be lower. With a lower vegetation cover, the soil is increasingly exposed, increasing the risk of desertification [48,49]. Thus, with a higher transfer of sensible heat flux, the air near the surface becomes warmer. The simulations we carried out showed that there was a more remarkable variability (excess of H and LE outliers) in the Cabrobó site, which might indicate that it is indeed a more unstable region regarding energy balance, compared with the Ibimirim site.

Water availability conditions also play an important role in the development of vegetation, and our results showed that rainfall distribution was indeed a limiting factor for productivity in the studied sites, which is consistent with previous studies found in the literature [20,21,50,51]. In one study [21], mean NEE values in the wet season of a preserved Caatinga site was -0.70 g C m^{-2} y^{-1}, while mean GPP was approximately 1.68 g C m^{-2} y^{-1}. In the dry season, NEE values increased to approximately -0.26 g C m^{-2} y^{-1}, while GPP values decreased to -0.64 g C m^{-2} y^{-1}. Mendes et al. [21] also compared the net ecosystem CO_2 exchange (NEE) of the Caatinga biome with that of other savannas and tropical forests across the globe, showing that Caatinga could be considered mostly a carbon sink with mean assimilation of -157 g C m^{-2} y^{-1} in 2014 and 2015. The SITE model's simulated results obtained in this study are similar to those found by Mendes et al. [21], especially in terms of the Cabrobó site results.

Therefore, our results indicate that the SITE model can reasonably simulate seasonal variations in CO_2 fluxes in the studied regions. Results showed that even in the dry season, the NEE over the studied sites presented negative values (controlled by CO_2 assimilation), indicating that the Caatinga biome acted as a carbon sink in 2009 and 2014. The reduction in GPP and NEE (near 0) values with the decrease in precipitation is closely related to the reduction in leaf cover. In turn, this reduction is linked to leaf senescence of the Caatinga vegetation, which is a resilience mechanism in the face of drought that limits photosynthetic activity to the few semideciduous species that manage to keep their leaves all year round.

During the dry season, trees are gradually impacted by the reduction in soil water content, which leads to the closure of stomates and to the reduction in stomatal conductance and leaf transpiration, which, in turn, limits CO_2 assimilation and reduces net photosynthesis.

The simulated values of the energy balance components agree with results from other studies carried out in Caatinga [24,52]. This provides further evidence that the SITE model is capable of simulating the partitioning of available energy into sensible and latent heat fluxes. For example, Campos [24] assessed the seasonal and annual behavior of energy partitioning and the energy balance closure in Caatinga. The authors identified a remarkable seasonal variability in the partitioning. Furthermore, they observed that during the dry period, more than half of the net radiation was converted into H, while in the wet season, this proportion reduced to less than 50%.

In the study carried out by Dos Santos et al. [52], the dry and wet seasons in the Caatinga region were analyzed. The authors observed that the conversion of energy into H is more expressive during the dry season. Mean LE values, on the other hand, reached approximately 200 W m^{-2} during the wet season, while in the dry season, it was nearly zero. This behavior was also explained by the closure of stomates and leaf senescence in most Caatinga plants as an adaptation to drier conditions, reducing water loss through transpiration. Furthermore, the authors observed that H, instead of LE, is the main driver of energy balance in the biome during drought years, mostly due to deficits in soil water availability, which lead to low photosynthetic activity.

Other studies compared densely vegetated Caatinga sites with other sites with more sparsely and heterogeneous vegetation cover [53]. Results of these studies show that most parts of the net radiation were converted into H, as expected in semiarid environments. In these regions, LE surpassed H during the wet season, while the inverse occurred in the dry season. Furthermore, the difference in H and LE values during the dry season was more noticeable among studied sites. Additionally, LE was higher and more intense in the densely vegetated Caatinga region.

Low LE values in the Caatinga region may also represent a defense mechanism by plants, associated with leaf loss, which can be indirectly measured by remotely sensed vegetation indices such as the normalized difference vegetation index (NDVI). Deforestation affects the relationship between rainfall and NDVI [54], with degraded lands presenting lower productivity even in high water availability conditions. In preserved areas, however, NDVI responds more smoothly to rainfall variability, remaining relatively high even in drier conditions, compared with degraded lands.

5. Conclusions

We investigated seasonal and annual patterns for the components of energy and CO_2 balances during a wet (2009) and a dry (2014) year in a site (Cabrobó) known as a desertification hotspot in Northeast Brazil using biophysical soil–vegetation–atmosphere transfer and compared the observed trends with those recorded in a site (Ibimirim) in the same area but outside the hotspot. We found an increasing air temperature trend in the Cabrobó site, mainly during the night, which was not observed as remarkably in the Ibimirim site. Overall, there was an increasing air temperature trend in the Cabrobó site, mainly during the night, which was not observed as remarkably in the Ibimirim site. Regarding relative humidity, no trends were observed in the first semester. However, a few increasing trends were observed in the Cabrobó site (particularly in November), while decreasing trends were observed in Ibimirim (mainly in August). Wind speed series presented an increasing trend in the Cabrobó site from June to August, while the opposite was observed in Ibimirim from September to May.

Sensible heat fluxes, latent heat fluxes, GPP, and NEE were satisfactorily simulated by the SITE model. GPP values were higher in the first half of the year in Ibimirim and Cabrobó, indicating that the CO_2 balance dynamics in Caatinga are closely linked to rainfall seasonality. NEE values were mostly negative throughout the year, indicating a higher CO_2 uptake even though minimum values were registered during dry months due to the lack

of soil water. The results of this study show that the SITE model can be used to simulate adequate responses of energy and CO_2 fluxes for the Caatinga region, considering the remarkable phenological seasonality of this biome.

Author Contributions: Conceptualization, A.C.S., C.M.S.e.S. and K.R.M.; methodology, A.C.S., C.M.S.e.S. and K.R.M.; validation, A.C.S., C.M.S.e.S., K.R.M., D.T.R. and P.R.M.; analyses formal A.C.S., C.M.S.e.S., K.R.M., D.T.R., P.R.M., R.R.F. and B.G.B.; investigation A.C.S., C.M.S.e.S. and K.R.M.; writing—original draft preparation, A.C.S., C.M.S.e.S. and K.R.M.; writing—review and editing, A.C.S., C.M.S.e.S., K.R.M., D.T.R., G.B.C., D.T.C.d.S., P.R.M., R.R.F. and B.G.B. All authors have read and agreed to the published version of the manuscript.

Funding: This research was funded by National Council for Scientific and Technological Development (CNPq), Process N°310781/2020-5 and National Observatory of Water and Carbon Dynamics in the Caatinga Biome (INCT-MCTI/CNPq/CAPES/FAPs 16/2014, grant: 465764/2014-2 and MCTI/CNPq N° 28/2018, grant 420854/2018-5).

Institutional Review Board Statement: Not applicable.

Informed Consent Statement: Not applicable.

Data Availability Statement: The data presented in this study are available on request from the corresponding author. The data are not publicly available due to privacy.

Acknowledgments: The authors are thankful to the Brazilian National Institute of Semi-Arid (INSA) for funding the project and providing the EC data used in this study. The authors are also thankful to the Coordination for the Improvement of Higher Education Personnel (CAPES) for the postdoctoral funding granted to the second author. This work was partially supported by the high-performance computing facilities of NPAD/UFRN. Finally, we are thankful to the National Council for Scientific and Technological Development (CNPq) for the research productivity grant of the C.M.S.eS. author (Process N° 310781/2020-5) and the financial support in the NOWCDCB project: National Observatory of Water and Carbon Dynamics in the Caatinga Biome (INCT-MCTI/CNPq/CAPES/FAPs 16/2014, Grant: 465764/2014-2 and MCTI/CNPq N° 28/2018, Grant 420854/2018-5).

Conflicts of Interest: The authors declare no conflict of interest.

References

1. UNCCD. *United Nations Convention to Combat Desertification in Countries Experiencing Serious Drought and/or Desertification, Particularly in Africa*; United Nations Convention to Combat Desertification (UNCCD): Paris, France, 1994; Chapter XXVII.
2. Mutti, P.R.; Lúcio, P.S.; Dubreuil, V.; Bezerra, B.G. NDVI time series stochastic models for the forecast of vegetation dynamics over desertification hotspots. *Int. J. Remote Sens.* **2019**, *41*, 2759–2788. [CrossRef]
3. Xu, D.; You, X.; Xia, C. Assessing the spatial-temporal pattern and evolution of areas sensitive to land desertification in North China. *Ecol. Indic.* **2019**, *97*, 150–158. [CrossRef]
4. Vieira, R.M.D.S.P.; Tomasella, J.; Barbosa, A.A.; Martins, M.; Rodriguez, D.; Rezende, F.; Carriello, F.; Santana, M.D. Desertification risk assessment in Northeast Brazil: Current trends and future scenarios. *Land Degrad. Dev.* **2021**, *32*, 224–240. [CrossRef]
5. Simplício, A.A.F.; Costa, C.A.G.; Hevia, J.N.; Araújo, J.C. Erosion at hillslope and micro-basin scales in the Gilbués desertification region, Northeastern Brazil. *Land Degrad. Dev.* **2021**, *32*, 1487–1499. [CrossRef]
6. Cunha, A.P.M.; Alvalá, R.C.; Nobre, C.A.; Carvalho, M.A. Monitoring vegetative drought dynamics in the Brazilian semiarid region. *Agric. For. Meteorol.* **2015**, *214–215*, 494–505. [CrossRef]
7. Mariano, D.A.; Santos, C.A.C.; Wardlow, B.D.; Anderson, M.; Schiltmeyer, A.V.; Tadesse, T.; Svoboda, M.D. Use of remote sensing indicators to assess effects of drought and human-induced land degradation on ecosystem health in Northeastern Brazil. *Remote Sens. Environ.* **2018**, *213*, 129–143. [CrossRef]
8. Huang, J.; Ji, M.; Xie, Y.; Wang, S.; He, Y.; Ran, J. Global semi-arid climate change over last 60 years. *Clim. Dyn.* **2016**, *46*, 1131–1150. [CrossRef]
9. Arellano-Sota, C. UNEP—Program on desertification control in Latin America and the Caribbean. *Desertif. Control. Bull.* **1996**, *29*, 56–62.
10. Mutti, P.R.; Dubreuil, V.; Bezerra, B.G.; Arvor, D.; De Oliveira, C.P.; Santos e Silva, C.M. Assessment of Gridded CRU TS Data for Long-Term Climatic Water Balance Monitoring over the São Francisco Watershed, Brazil. *Atmosphere* **2020**, *11*, 1207. [CrossRef]
11. Dubreuil, V.; Fante, K.P.; Planchon, O.; Neto, J.L.S. Climate change evidence in Brazil from Köppen's climate annual types frequency. *Int. J. Clim.* **2019**, *39*, 1446–1456. [CrossRef]
12. Marengo, J.A.; Torres, R.R.; Alves, L.M. Drought in Northeast Brazil—past, present, and future. *Theor. Appl. Clim.* **2017**, *129*, 1189–1200. [CrossRef]

13. Tomasella, J.; Silva, P.V.R.M.; Barbosa, A.A.; Rodriguez, D.A.; Oliveira, S.; Marcos, D.; Sestini, M.F. Desertification trends in the Northeast of Brazil over the period 2000–2016. *Int. J. Appl. Earth Obs. Geoinf.* **2018**, *73*, 197–206. [CrossRef]
14. Koch, R.; Almeida-Cortez, J.S.; Kleinschmit, B. Revealing areas of high nature conservation importance in a seasonally dry tropical forest in Brazil: Combination of modelled plant diversity hot spots and threat patterns. *J. Nat. Conserv.* **2017**, *35*, 24–39. [CrossRef]
15. Tang, Z.; An, H.; Deng, L.; Wang, Y.; Zhu, G.; Shangguan, Z. Effect of desertification on productivity in a desert steppe. *Sci. Rep.* **2016**, *6*, 27839. [CrossRef] [PubMed]
16. Mahecha, M.D.; Reichstein, M.; Lange, H.; Carvalhais, N.; Bernhofer, C.; Grünwald, T.; Papale, D.; Seufert, G. Characterizing ecosystem-atmosphere interactions from short to interannual time scales. *Biogeosciences* **2007**, *4*, 743–758. [CrossRef]
17. Marcolla, B.; Rödenbeck, C.; Cescatti, A. Patterns and controls of inter-annual variability in the terrestrial carbon budget. *Biogeosciences* **2017**, *14*, 3815–3829. [CrossRef]
18. Wohlfahrt, G.; Hammerle, A.; Haslwanter, A.; Bahn, M.; Tappeiner, U.; Cernusca, A. Seasonal and inter-annual variability of the net ecosystem CO_2 exchange of a temperate mountain grassland: Effects of weather and management. *J. Geophys. Res.* **2008**, *113*, 113. [CrossRef]
19. Ahlström, A.; Raupach, M.R.; Schurgers, G.; Smith, B.; Arneth, A.; Jung, M.; Reichstein, M.; Canadell, J.G.; Friedlingstein, P.; Jain, A.K.; et al. The dominant role of semi-arid ecosystems in the trend and variability of the land CO_2 sink. *Science* **2015**, *348*, 895–899. [CrossRef]
20. Silva, P.F.; Lima, J.R.D.S.; Antonino, A.C.D.; Souza, R.; de Souza, E.S.; Silva, J.R.; Alves, E.M. Seasonal patterns of carbon dioxide, water and energy fluxes over the Caatinga and grassland in the semi-arid region of Brazil. *J. Arid. Environ.* **2017**, *147*, 71–82. [CrossRef]
21. Mendes, K.R.; Campos, S.; Da Silva, L.L.; Mutti, P.R.; Ferreira, R.R.; Medeiros, S.S.; Perez-Marin, A.M.; Marques, T.V.; Ramos, T.M.; Vieira, M.M.D.L.; et al. Seasonal variation in net ecosystem CO_2 exchange of a Brazilian seasonally dry tropical forest. *Sci. Rep.* **2020**, *10*, 9454. [CrossRef]
22. Baldocchi, D.D.; Law, B.E.; Anthoni, P.M. On measuring and modeling energy fluxes above the floor of a homogeneous and heterogeneous conifer forest. *Agric. For. Meteorol.* **2000**, *102*, 187–206. [CrossRef]
23. Baldocchi, D.; Falge, E.; Gu, L.H.; Olson, R.; Hollinger, D.; Running, S.; Anthoni, P.; Bernhofer, C.; Davis, K.; Evans, R.; et al. FLUXNET: A new tool to study the temporal and spatial variability of ecosystem-scale carbon dioxide, water vapor, and energy flux densities. *Bull. Am. Meteorol. Soc.* **2001**, *82*, 2415–2434. [CrossRef]
24. Campos, S. Closure and partitioning of the energy balance in a preserved area of a Brazilian seasonally dry tropical forest. *Agric. For. Meteorol.* **2019**, *271*, 398–412. [CrossRef]
25. Arraes, F.D.D.; De Andrade, E.M.; Da Silva, B.B. Dinâmica do balanço de energia sobre o açude Orós e suas adjacências. *Rev. Caatinga* **2012**, *25*, 119–127. Available online: https://www.redalyc.org/articulo.oa?id=237123860018 (accessed on 6 November 2020).
26. Beer, C. Terrestrial gross carbon dioxide uptake: Global distribution and covariation with climate. *Science* **2010**, *329*, 834–838. [CrossRef]
27. Cleverly, J. Productivity and evapotranspiration of two contrasting semiarid ecosystems following the 2011 global carbon land sink anomaly. *Agric. For. Meteorol.* **2016**, *220*, 151–159. [CrossRef]
28. Tang, X.; Carvalhais, N.; Moura, C.; Ahrens, B.; Koirala, S.; Fan, S.; Guan, F.; Zhang, W.; Gao, S.; Magliulo, V.; et al. Global variability of carbon use efficiency in terrestrial ecosystems. *Biogeosci. Discuss.* **2019**. [CrossRef]
29. Von Randow, C.; Zeri, M.; Restrepo-Coupe, N.; Muza, M.N.; de Gonçalves, L.G.G.; Costa, M.H.; Araujo, A.C.; Manzi, A.O.; da Rocha, H.R.; Saleska, S.R.; et al. Inter-annual variability of carbon and water fluxes in Amazonian forest, Cerrado and pasture sites, as simulated by terrestrial biosphere models. *Agric. For. Meteorol.* **2013**, *182*, 145–155. [CrossRef]
30. Marques, T.V. Mecanismos Biofísicos e Características de Controle da Evapotranspiração da Caatinga em anos de seca Extrema. Tese (Doutorado em Ciências Climáticas)—Centro de Ciências Exatas e da Terra, Universidade Federal do Rio Grande do Norte. 2020. Available online: https://repositorio.ufrn.br/handle/123456789/29714 (accessed on 12 October 2020).
31. Mendes, K.R.; Campos, S.; Mutti, P.R.; Ferreira, R.R.; Ramos, T.M.; Marques, T.V.; Dos Reis, J.S.; Vieira, M.M.D.L.; Silva, A.C.N.; Marques, A.M.S.; et al. Assessment of SITE for CO_2 and Energy Fluxes Simulations in a Seasonally Dry Tropical Forest (Caatinga Ecosystem). *Forests* **2021**, *12*, 86. [CrossRef]
32. Ferreira, R.R.; Mutti, P.R.; Mendes, K.R.; Campos, S.; Marques, T.V.; Oliveira, C.P.; Gonçalves, W.; Mota, J.; Difante, G.; Urbano, S.A.; et al. An assessment of the MOD17A2 gross primary production product in the Caatinga biome, Brazil. *Int. J. Remote Sens.* **2021**, *42*, 1275–1291. [CrossRef]
33. Perez-Marin, A.M.; Cavalcante, A.D.M.B.; Medeiros, S.S.D.; Tinôco, L.B.D.M.; Salcedo, I.H. Núcleos de desertificação do semiárido brasileiro: Ocorrência natural ou antrópica? *Parcerias Estratégicas* **2013**, *17*, 87–106.
34. Santos, S.N.M.; Costa, M.H. A simple tropical ecosystem model of carbon, water and energy fluxes. *Ecol. Model.* **2004**, *176*, 291–312. [CrossRef]
35. Vianello, R.L.; Alves, A.R. *Meteorologia Básica e Aplicações 2*; Viçosa, M.G., Ed.; Universidade Federal de Viçosa: Vicosa, Brazil, 2012.
36. Idso, S.B. A set of equations for full spectrum and 8-to 14-μm and 10.5-to 12.5-μm thermal radiation from cloudless skies. *Water Resour. Res.* **1981**, *17*, 295–304. [CrossRef]

37. Prata, A.J. A new long-wave formula for estimating downward clear-sky radiation at the surface. *Q. J. R. Meteorol. Soc.* **1996**, *122*, 1127–1151. [CrossRef]
38. Santos, C.A.C.; Da Silva, B.B.; Rao, T.V.R.; Satyamurty, P.; Manzi, A.O. Downward longwave radiation estimates for clear-sky conditions over northeast Brazil. *Rev. Bras. Meteorol.* **2011**, *26*, 443–450. [CrossRef]
39. Silva, J.B.; Gaio, D.C.; Curado, L.F.A.; Nogueira, J.D.S.; Júnior, L.C.G.V.; Rodrigues, T.R. Evaluation of methods for estimating atmospheric emissivity in Mato-Grossense Cerrado. *Ambient. Agua* **2019**, *14*. [CrossRef]
40. Oliveira, A.C.C.F.D.; Vieira, M.M.D.L.; Mendes, K.R.; Silva, C.M.S.; Bezerra, B.G. Estimativa da radiação de onda longa atmosférica sobre condições de céu claro na região Seridó. In Proceedings of the Simpósio Internacional de Climatologia, VII, Anais do VIII Simpósio Internacional de Climatologia, Belém, Brasil, 12 November 2019.
41. Mann, H.B. Nonparametric Tests Against Trend. *Econom. J. Econ. Soc.* **1945**, *13*, 245–259. [CrossRef]
42. Kendall, M.G. *Rank Correlation Methods*; Charles Griffin: London, UK, 1975; p. 120.
43. Wang, F.; Shao, W.; Yu, H.; Kan, G.; He, X.; Zhang, D.; Ren, M.; Wang, G. Re-evaluation of the Power of the Mann-Kendall Test for Detecting Monotonic Trends in Hydrometeorological Time Series. *Front. Earth Sci.* **2020**, *8*, 14. [CrossRef]
44. Gilbert, R.O. *Statistical Methods for Environmental Pollution Monitoring*; John Wiley & Sons: Hoboken, NJ, USA, 1987.
45. Chambers, J.M.; Cleveland, W.S.; Kleiner, B.; Tukey, P.A. *Graphical Methods for Data Analysis*; CRC Press Taylor & Francis Group: Boca Raton, FL, USA, 1983.
46. R Core Team. *R: A Language and Environment for Statistical Computing*; R Foundation for Statistical Computing: Vienna, Austria, 2015; Available online: https://www.gbif.org/tool/81287/r-a-language-and-environment-for-statistical-computing (accessed on 20 October 2020).
47. Wickham, H.; Chang, W.; Wickham, M.H. Package 'ggplot2'. Create Elegant Data Visualisations Using the Grammar of Graphics. *Version* **2016**, *2*, 1–189.
48. Li, X.-Y.; Liu, L.-Y.; Wang, J.-H. Wind tunnel simulation of aeolian sandy soil erodibility under human disturbance. *Geomorphology* **2004**, *59*, 3–11. [CrossRef]
49. Lin, Y.; Han, G.; Zhao, M.; Chang, S.X. Spatial vegetation patterns as early signs of desertification: A case study of a desert steppe in Inner Mongolia, China. *Landsc. Ecol.* **2010**, *25*, 1519–1527. [CrossRef]
50. Ma, X.; Huete, A.; Cleverly, J.; Eamus, D.; Chevallier, F.; Joiner, J.; Poulter, B.; Zhang, Y.; Guanter, L.; Meyer, W.; et al. Drought rapidly diminishes the large net CO_2 uptake in 2011 over semi-arid Australia. *Sci. Rep.* **2016**, *6*, 37747. [CrossRef]
51. Arruda, P.H.; Vourlitis, G.; Santanna, F.B.; Pinto-Junior, O.B. Large net CO_2 loss from a grass-dominated tropical savanna in south-central Brazil in response to seasonal and interannual drought. *J. Geophys. Res. Biogeosci.* **2016**, *121*, 2110–2124. [CrossRef]
52. Dos Santos, C.A.C.; Mariano, D.A.; Nascimento, F.D.C.A.D.; Dantas, F.R.D.C.; de Oliveira, G.; Silva, M.T.; da Silva, L.L.; da Silva, B.B.; Bezerra, B.; Safa, B.; et al. Spatio-temporal patterns of energy exchange and evapotranspiration during an intense drought for drylands in Brazil. *Int. J. Appl. Earth Obs. Geoinf.* **2020**, *85*, 101982. [CrossRef]
53. Borges, C.K.; Santos, C.A.C.; Carneiro, R.G.; Silva, L.L.; Oliveira, G.; Mariano, D.; Silva, M.T.; Da Silva, B.B.; Bezerra, B.G.; Perez-Marin, A.M.; et al. Seasonal variation of surface radiation and energy balances over two contrasting areas of the seasonally dry tropical forest (Caatinga) in the Brazilian semi-arid. *Environ. Monit. Assess.* **2020**, *192*, 524. [CrossRef] [PubMed]
54. Salvatierra, L.H.A.; Ladle, R.J.; Barbosa, H.; Correia, R.A.; Malhado, A.C.M. Protected areas buffer the Brazilian semi-arid biome from climate change. *Biotropica* **2017**, *49*, 753–760. [CrossRef]